

Dalton Transactions

Accepted Manuscript



This is an *Accepted Manuscript*, which has been through the Royal Society of Chemistry peer review process and has been accepted for publication.

Accepted Manuscripts are published online shortly after acceptance, before technical editing, formatting and proof reading. Using this free service, authors can make their results available to the community, in citable form, before we publish the edited article. We will replace this *Accepted Manuscript* with the edited and formatted *Advance Article* as soon as it is available.

You can find more information about *Accepted Manuscripts* in the [Information for Authors](#).

Please note that technical editing may introduce minor changes to the text and/or graphics, which may alter content. The journal's standard [Terms & Conditions](#) and the [Ethical guidelines](#) still apply. In no event shall the Royal Society of Chemistry be held responsible for any errors or omissions in this *Accepted Manuscript* or any consequences arising from the use of any information it contains.

ARTICLE

Benzo annulated cycloheptatriene PCP Pincer Iridium complexes

Cite this: DOI: 10.1039/x0xx00000x

Wolfgang Leis^a, Sophie Wernitz^a, Benedikt Reichart^b, David Ruckerbauer^b, Johannes Wolfram Wielandt^{*b} and Hermann A. Mayer^{*a}

Received 00th January 2012,
Accepted 00th January 2012

DOI: 10.1039/x0xx00000x

www.rsc.org/

The benzo annulated cycloheptatriene PCP pincer ligand **5** was prepared in five steps. Treatment of **5** with Ir(CO)₃Cl gave the meridional cyclometalated chlorohydrido carbonyl iridium complexes **6a-c** which differ in their arrangement of the H, Cl, and CO ligands around iridium. Storing **6** in THF led to isomerization processes. Hydrogen shifts from the sp³-CH carbon bound to iridium into the ligand backbone produced the three isomers **7a-c**. Reductive elimination of HCl from these complexes resulted in the square planar Ir(I) carbonyl complexes **8a-c**. Abstraction of the hydrogen from the sp³-CH-Ir fragment could be achieved either by treatment of **6** with Ph₃CBF₄ or by the elimination of H₂ which is initiated by CF₃SO₃H. The mass spectrometric characterisation of **6** using fast atom bombardment reveals a complex fragmentation pattern. These different "fragment" ions were further investigated by electro-spray ionisation (tandem) mass spectrometry in high and low resolution. The identified compounds were attributed to structures by DFT calculations.

Introduction

Rational ligand design in pincer complex chemistry has created a huge library of multifunctional building blocks with broad applications ranging from homogeneous catalysis to biomarkers for medical diagnostics.¹⁻⁸ Typical features associated with pincer complexes are a well balanced stability versus reactivity, high efficiency and selectivity combined with functional group tolerance. In recent years cooperation of some pincer ligands with the coordination centre have been reported.⁹⁻¹² In the course of this process the ligands undergo reversible structural changes during the activation of a substrate and while forming the products. In this way the scope of pincer complex chemistry has been expanded. This has been demonstrated in a number of stoichiometric reactions^{13,14} and catalytic transformations.^{15,16} In these cases the metal ligand cooperation acts *via* dearomatisation and aromatisation steps of the ligand backbone,¹⁷ which is facilitated by the acidic protons of the ring methylene groups and the ability of nitrogen to offer different binding modes to the metal centre.

The chemistry of the CHT PCP pincer complexes (CHT PCP = 1,6-bis(methylene (di-*tert*-butyl phosphine) cycloheptatriene) is dominated by the acidic methylene protons and the possibility to form an aromatic tropylium cation.¹⁸⁻²¹ This leads to an easy interconversion between several complexes of different ligand structure and/or metal oxidation states. Several unusual reactions have been reported e.g. abstraction of a hydride from the ligand backbone in the presence of a metal hydride¹⁹ as well as the shift of two hydrides from the metal into the ligand

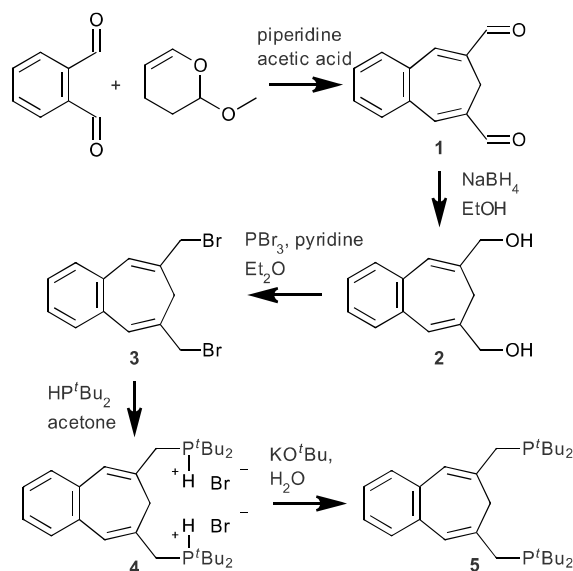
backbone.²⁰ In order to extend this chemistry we have prepared a benzo annulated cycloheptatriene PCP pincer ligand (Scheme 1) and studied the chemistry of the corresponding iridium complexes.

Mass spectrometry (MS) with field desorption (FD)²²⁻²⁴ or fast atom bombardment (FAB)²⁵⁻²⁹ ion sources are well established characterization techniques for organometallic compounds. Electro-spray ionization (ESI)³⁰⁻³² as a very soft ionization technique has proven to be a very versatile tool in characterization of ionic or easily ionisable compounds³³. Especially peptides but also inorganic or organometallic compounds^{34,35} were investigated. The application of ESI-MS to air and or water sensitive compounds is more tricky because the transfer of the sample via syringe, syringe pump and transfer-capillary to the ionization chamber. A recent overcome for this drawback is to couple a glove-box with syringe pump inside via a transfer-capillary to the ESI chamber.³⁶

Results and Discussion

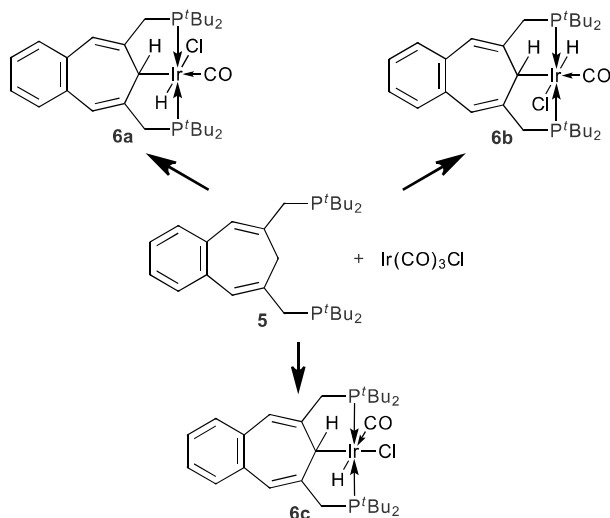
The preparation of the benzo cycloheptatriene (BCHT) PCP ligand **5** succeeds in good yield as outlined in Scheme 1. Starting from commercially available phthalic dialdehyde and dihydro methoxy pyrane the benzo cycloheptatriene dialdehyde **1** is obtained via an acid catalysed double aldol reaction as previously described.³⁷ Subsequent reduction of the dialdehyde **1** with sodium boron-hydride followed by bromination with PBr₃ (see supplementary information) afforded the diol **2** and the dibromide **3**. The conversion of **3**

into **5** was achieved by the addition of di-*tert* butylphosphine and consecutive deprotonation of the isolated bisphosphonium dibromide **4**.



Scheme 1

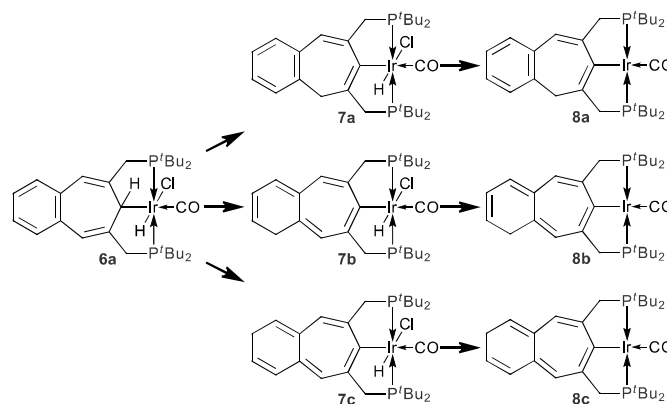
All NMR spectra are in agreement with the C_s/C_2 symmetric structure as displayed in Scheme 1. Characteristic features are a singlet at δ_p 16.1 in the $^{31}\text{P}\{^1\text{H}\}$ NMR spectrum and a triplet at δ_H 2.76 ($^4J_{\text{PH}} = 1.3$ Hz) in the ^1H NMR spectrum for the methylene group belonging to the cycloheptatriene ring. This indicates that at room temperature a fast flip of the CH_2 group between two possible conformers is operative. Overall the chemical shifts of the novel BCHT PCP ligand **5** are very similar to the corresponding shifts of the CHT PCP ligand.¹⁸



Scheme 2

After treatment of the BCHT PCP ligand **5** with $\text{Ir}(\text{CO})_3\text{Cl}$ in THF at slightly elevated temperatures a yellow to orange residue was isolated which gave three singlets in the $^{31}\text{P}\{^1\text{H}\}$ NMR spectrum. The resonances at δ_p 61.5, 49.0 and 46.0

integrate to 1 : 15 : 3. Based on homo- and hetero-nuclear two dimensional NMR spectroscopy all resonances could be unambiguously assigned to the three isomers **6a-c** which differ only in their arrangement of the H, Cl, and CO ligands around iridium (Scheme 2). For instance the hydride chemical shifts of compounds **6a** and **6b** at δ_H -17.77 and -18.85, respectively, are typical for hydrogens located *trans* to a ligand with a weak *trans*-influence.³⁸ Isomer **6b** is then identified by a cross peak due to the correlation of the hydride resonance with the *ipso*-C-H proton signal in the $^1\text{H}, ^1\text{H}$ NOESY spectrum while for **6a** and **6c** no such correlations are observed. Isomer **6c** is distinguished from **6b** by the hydride chemical shift of -10.09 ppm which is characteristic for hydrogens located *trans* to ligands with a strong *trans*-influence. The observation of one set of resonances for the $^t\text{Bu}_2\text{P}$ groups in the ^1H , ^{13}C and ^{31}P NMR spectra is in agreement with a C_s/C_2 symmetry for all three isomers. Different attempts to separate the isomer mixture by recrystallisation led to decomposition of **6** or backbone rearrangements according to Scheme 3.



Scheme 3

If a sample of **6** is stored in THF for two days at room temperature (and light) further isomerisation processes took place which are followed by reductive elimination of hydrochloric acid (Scheme 3). This could be deduced from a two dimensional $^{31}\text{P}, ^{31}\text{P}$ COSY experiment (Figure 1) and by comparison with the more detailed investigations of backbone rearrangements in the analogous CHT iridium pincer complexes.^{19,20,39} In the $^{31}\text{P}\{^1\text{H}\}, ^{31}\text{P}\{^1\text{H}\}$ COSY NMR spectrum two characteristic chemical shift domains for the Ir(III) (**7a-c**) at higher fields and Ir(I) (**8a-c**) complexes at lower fields can be identified which are covered by three AB patterns each. The observed $^2J_{\text{PP}}$ coupling constants between 250 and 350 Hz agree well with the mutual *trans* arrangements of the phosphorous groups in **7a-c** and **8a-c**. Unfortunately a more precise attribution of the resonances was not achieved due to problems in separating single components. The rearrangements are a consequence of the higher stability of the sp^2 C-Ir as compared to the sp^3 C-Ir bond.²⁰

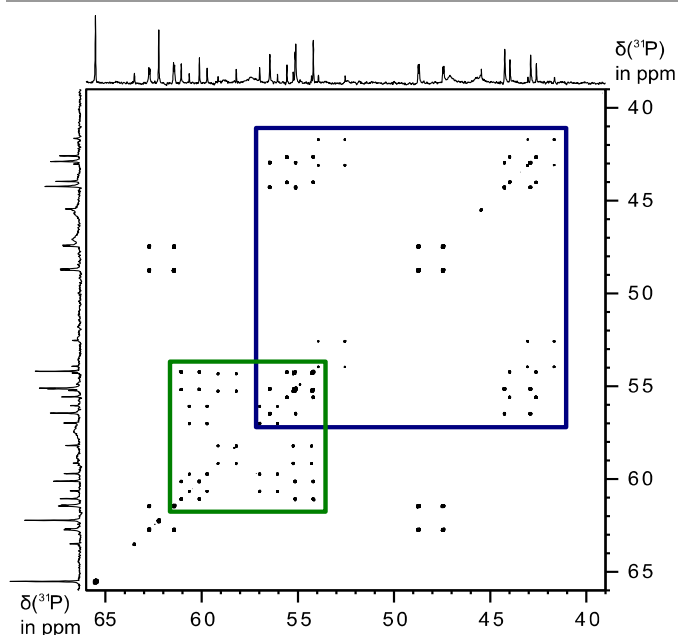
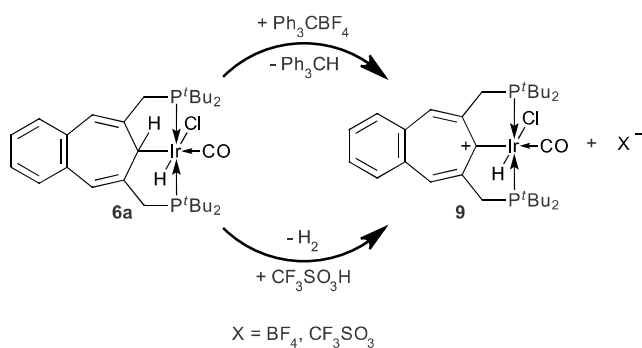


Figure 1: Proton decoupled ^{31}P , ^{31}P COSY NMR spectrum of **6** after 2 days in THF solution.

As previously described for the analogous CHT Ir complex the abstraction of the hydride from the *ipso*-carbon atom in the hydrido chloro complexes **6** is achieved with trimethylsilyl triflate^{19,39} or using triphenylcarbenium tetrafluoroborate. The resulting cationic complex **9** may alternatively be obtained by treatment of **6** in DCM with equimolar amounts of dry triflic acid.



Scheme 4

This cationic Ir(III) complex **9** is extensively characterised by multi-nuclear 1D and 2D NMR spectroscopy as well as mass spectrometry. In the low temperature $^{31}\text{P}\{^1\text{H}\}$ NMR spectra of a solution of **6a** and triphenylcarbenium tetrafluoroborate in DCM- d_2 an intermediate species could be observed. The spectrum at -60°C displays a singlet each for the uncharged complex **6a** at 49.0 ppm, and the cationic product **9** at 60.5 ppm (Scheme 4) as well as an AB-pattern at 45.2 and -63.4 ppm with an AB-coupling constant of 231.8 Hz. This large P-P-coupling constant is evident for a mutual *trans*-orientation of the phosphorus nuclei at the metal while the great chemical shift difference of 108.6 ppm speaks for a strong change in the

electronic surrounding of one of the phosphorus nuclei. In the corresponding ^1H NMR spectrum three hydride signals are observed two triplets associated with the reagent **6a** at -19.12 ppm and the product **9** at -17.07 ppm and a broad multiplet at -14.68 ppm. The $^{13}\text{C}\{^1\text{H}\}$ data at room temperature displays the characteristic shift of the resonance of the *ipso*-carbon atom in **6a** at 42.8 ppm to 228.2 ppm in **9**. A further characterisation of the asymmetric intermediate was not achieved due to its low concentration in the mixture. These observations are in contradiction to a concerted formation of the triphenylmethane and **9**. Therefore a multi-step mechanism is proposed involving the formation of a less symmetric cationic intermediate whose structure remains still unclear. Crystals of **9**· BF_4 suitable for XRD analysis could be isolated from a crude reaction mixture in DCM. Unfortunately, these crystallographic data contain significant amounts of residual electron density after refinement (see Table S3 supplementary information).

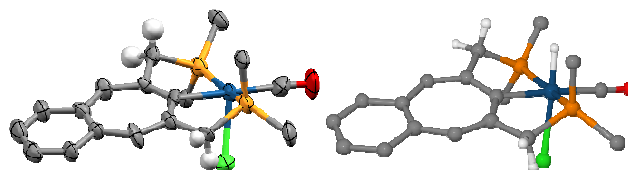


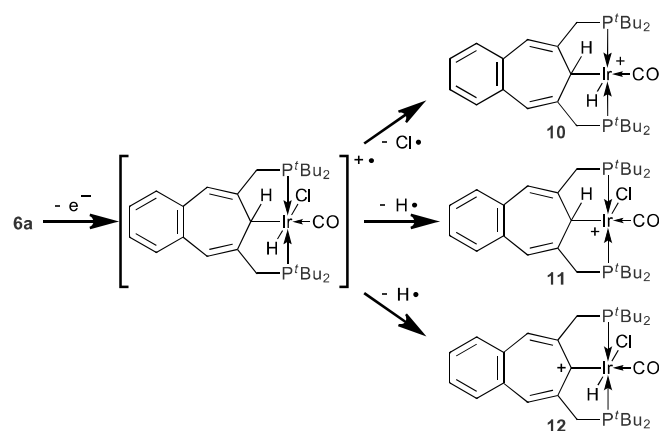
Figure 2: Left, single crystal XRD structure of **9**. Right, structure of **9** from geometry optimisation (B3LYP/LACVP*). The methyl groups, aromatic hydrogen and the tetrafluoroborate counter-ion (on the left) are omitted for clarity.

Probably, this is attributed to disordered dichloromethane which could not be refined successfully. However, the connections in the cationic complex could be clearly verified. Figure 2 shows the structure of **9** derived from crystallography and the respective quantum-mechanically optimised geometry. The cationic complex **9** is nearly C_2 symmetric and contains a planar BCHT backbone. The iridium chlorine bond length is with 250.8 (x-ray) and 253.8 pm (opt.) in the range of the previously described Ir-Cl bonds *trans* to the strong structural *trans*-effect ligand hydride (249.6 pm).¹⁹ The comparison of the experimental and the optimised structures of **9** reveal only slight differences. While the structural parameters of **9** are in very good agreement with the structure of the analogous CHT complex. The slight elongation of the Ir-CO bond accompanied by the slight shortening of the C-O and the Ir- C_{ipso} bond are indicative for increased π -backbonding into the π -system of the backbone. (see supplementary information, Table S1 and Table S2).

Mass spectrometry of benzocycloheptatriene complexes

IONISATION PROCESS OF **6A**

Due to the collision ionisation in a FAB source, the formation of higher energy intermediates as well as subsequent fragmentation is possibly observed. In contrast to this, higher energy intermediates can be avoided by the selectivity of the initial electrochemical oxidation in an electro-spray ionisation source. Consequently formation of fragments is expected to be minimal.



Scheme 5

A single electron oxidation process is assumed as the initial ionisation step for complex **6a** in electro-spray as well as in fast atom bombardment ionisation (Scheme 5). The resulting radical cation $[M]^{+\bullet}$ is not observed in the mass spectra. If $[M]^{+\bullet}$ emits a chlorine atom, the metal centred cation **10** is formed. The loss of a hydrogen atom from $[M]^{+\bullet}$ can proceed in two ways, either the removal of the hydrogen ligand from the metal (**11**) or the abstraction of the hydrogen from the metal bound carbon atom (**12**).

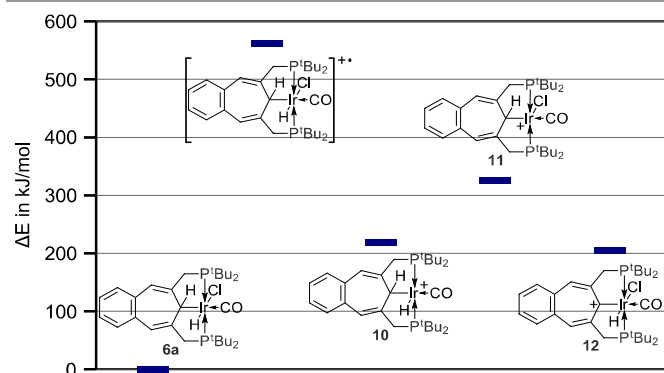
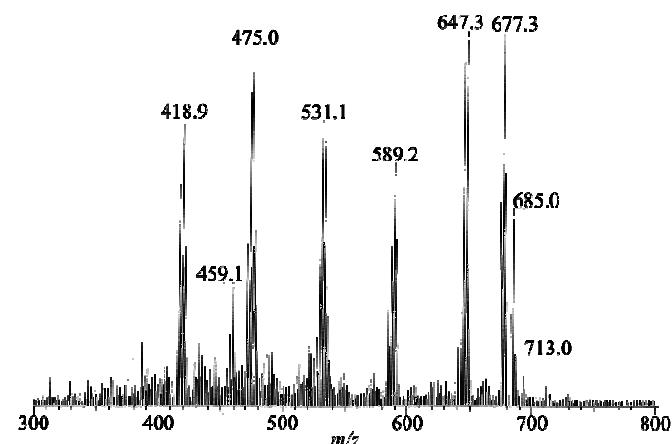
Figure 3: DFT energies of the species in Scheme 5 relative to the energy of **6a**.

Figure 3 shows the relative DFT energies of the different cationic structures. The formations of **10**, **11** and **12** from the radical cation $[M]^{+\bullet}$ are thermodynamically favoured with 341.8, 236.7 and 356.1 kJ/mol, respectively. Hence, a hydrogen atom from $[M]^{+\bullet}$ is preferentially eliminated from the *ipso*-carbon atom generating the aromatic compound **12**. While the emission of a chlorine atom from the radical cation $[M]^{+\bullet}$ is just 14.3 kJ/mol higher in energy than **10**.

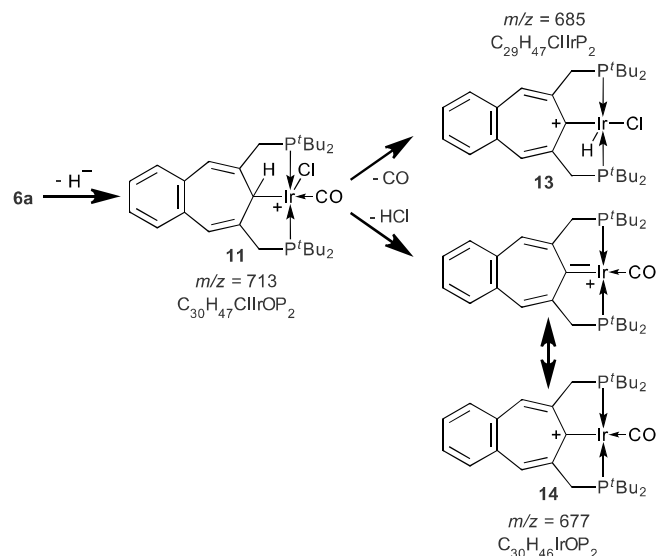
FAST ATOM BOMBARDMENT MASS SPECTROMETRY OF **6a**

The FAB mass spectrum of **6a** (Figure 4) in positive ion mode is measured in 3-nitro-benzyl alcohol as matrix. The obtained spectrum shows the molecular ion peak $[M-H]^+$ at m/z 713 with weak intensity which indicates the poor stability of this ion. From the two possible isomers of $[M-H]^+$, **11** and **12** (Scheme 5), isomer **12** is most likely the structure of the

$[M-H]^+$ ion as it is by 119.4 kJ/mol more stable than **11** (Figure 3).

Figure 4: FAB mass spectrum of **6a**

The following signals m/z 685 and 677 could be attributed to the structures **13** and **14**, respectively (Scheme 6). In complex **11** the positive charge is formally located on the metal centre. The hydrogen bound to the *ipso*-carbon and the chlorine are in a *syn*-periplanar orientation. This auspicious situation in **11** is a precondition for a uni-molecular HCl elimination process, forming the carbene resonance structure of **14** (m/z 677). Furthermore, **11** is able to emit carbon monoxide accompanied by the 1,2-hydride shift to the iridium centre leading to the m/z 685 attributed to **13**.



Scheme 6

Alternatively, **13** might be formed from complex **12**, by splitting the iridium carbonyl bond and rearranging the chloride *trans* to the *ipso*-carbon. As the cleavage of a strong carbonyl metal bond is involved in these reactions, the entire process appears to be kinetically less favourable. Independent of the

kinetic situation the generation of **13** and **14** from precursor **11** are driven by the formation of an aromatic backbone (Figure 5).

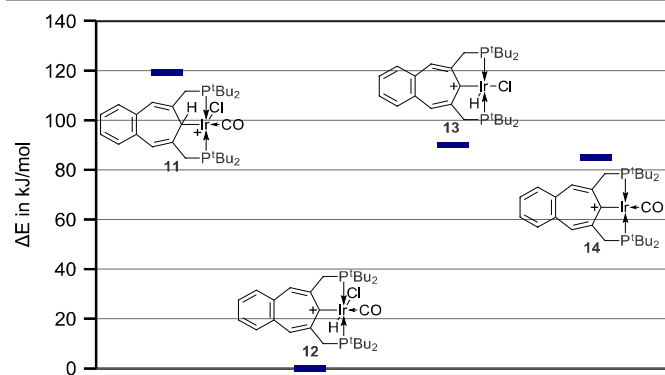


Figure 5: DFT energies of the species in Scheme 6 relative to the energy of **12**.

Energetically, the generation of the initial cations **11** from complex **6a** is a highly endergonic process as seen in Figure 3. Therefore the elimination of HCl or CO from **11** forms the complexes **13** and **14** which are stabilised by 29.3 kJ/mol and 34.6 kJ/mol, respectively (Scheme 6 and Figure 5). On the contrary, the removal of carbon monoxide from **12**, is by 90.2 kJ/mol endergonic and hence not expected to be operational in this case. The discussion of the remaining fragments in the FAB mass spectra follows in combination with the results of the ESI-MSⁿ measurements.

ELECTRO-SPRAY IONISATION MASS SPECTROMETRY OF **6a**

The assembly for routine direct infusion mass spectra with the Bruker Daltonics esquire3000plus spectrometer is depicted in the supplemental informations Figure S1.

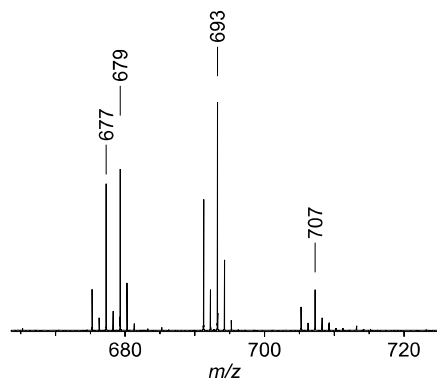
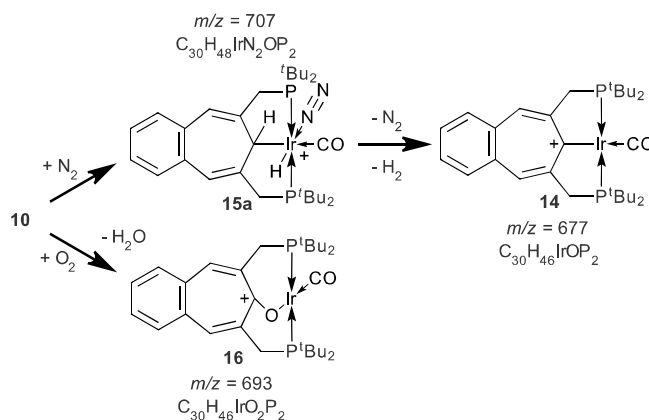


Figure 6: High resolution ESI mass spectrum of **6a** with routine infusion.

The mass analysis of **6a** with this routine set-up displays a mixture of four m/z signals with the typical isotope pattern of iridium $^{191}\text{Ir} : ^{193}\text{Ir} \approx 37 : 63$ (Figure 6). The intensity of the m/z signals 677 is enhanced, while m/z 707 decreases, with rising potentials of the transfer capillary exit (analogue to cone voltage). This behaviour is an indication for the fragmentation of m/z 707 in favour of m/z 677 in the ESI source or during the desolvation process. An increasing capillary exit potential results in higher collision energies between the desolvated ions and the drying gas (N_2) and consequently ion fragmentation may be observed in the spectra. High resolution mass

spectrometry (HRMS) with a Fourier transform ion-cyclotron-resonance (FTICR) instrument equipped with an ESI source and the routine infusion set-up (Figure S1) allowed the attribution of the m/z 677, 679, 693 and 707 to their sum formulas (Scheme 7).



Scheme 7

Hence, **15a** with m/z 707 could formally be explained by the loss of a chloride ion from **6a** and the subsequent coordination of dinitrogen. In Figure 7 the different geometry optimised isomers of the dinitrogen complex **15** are shown. The most stable structure ($\Delta(\Delta E) = -21.4$ kJ/mol relative to **10**) is **15d** with *syn*-periplanar orientation of the metal bound and the carbon bound hydrogen atoms.

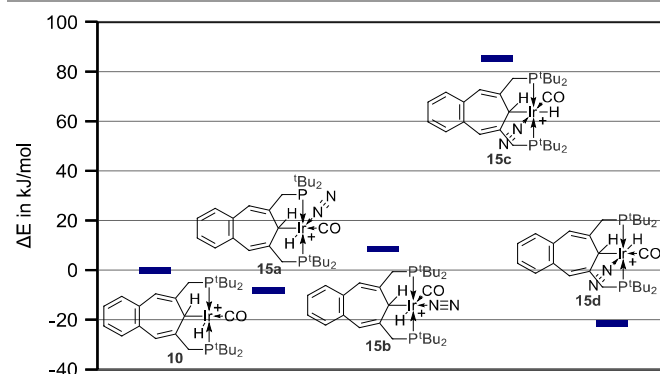


Figure 7: DFT energies of the different isomers of **15a** relative to the energy of **10**.

If the adduct is formed without any rearrangement at the metal centre, the resulting compound **15a** is 8 kJ/mol lower in energy than **10**. The remaining structures **15b** and **15c** with *syn*-periplanar arrangement of the carbon bound hydrogen atom and the carbon monoxide ligand are 8.7 and 85.4 kJ/mol less stable than **10**. Complex **14** with m/z 677 is 37.3 kJ/mol endergonic compared to **15a** and could be rationalised by the loss of a molecule of dihydrogen and dinitrogen from **15a** (Figure 8). Whereas m/z 679 (**10**) results just from chlorine abstraction from the initial radical cation $[\text{M}]^{\bullet+}$. The sum formula of **16** reveals an additional oxygen atom as compared to **14**. Therefore the structure of **16** is proposed in analogy to

the structure of the cycloheptatriene oxo-complex which was characterised by NMR spectroscopy and single crystal XRD.³⁹

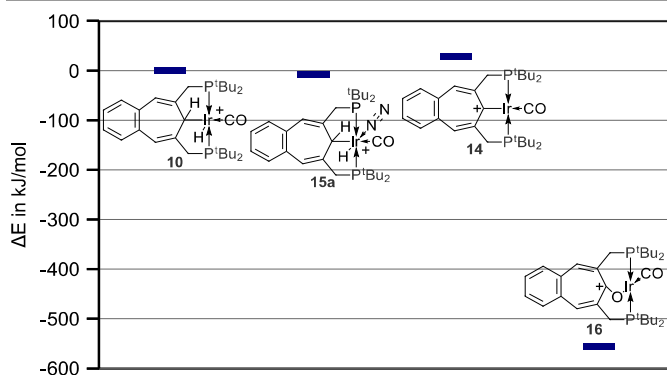


Figure 8: DFT energies of the species in Scheme 7 relative to the energy of **10**.

There are similar iridium and rhodium complexes known featuring bridging oxo pincer ligands, which were accessed from their phenol ligand precursors.^{40,41} The formation of compound **16** is unexpected because an oxygen donor (O_2 or H_2O) is required and the application of the routine set-up should avoid higher concentrations of oxygen or water in the sample solution. In order to locate the oxygen source an improved direct infusion set-up was developed which effectively avoids the contact between the sample solution and the atmosphere (see Figure S2 in the supplemental information).

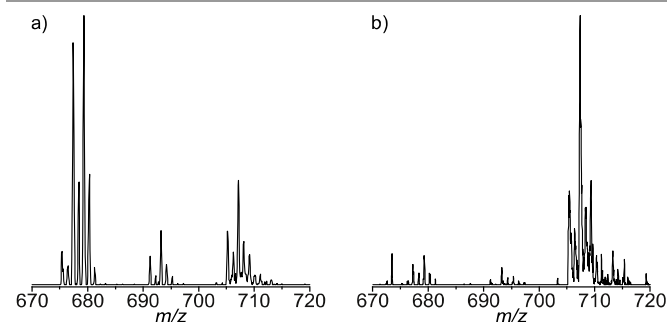


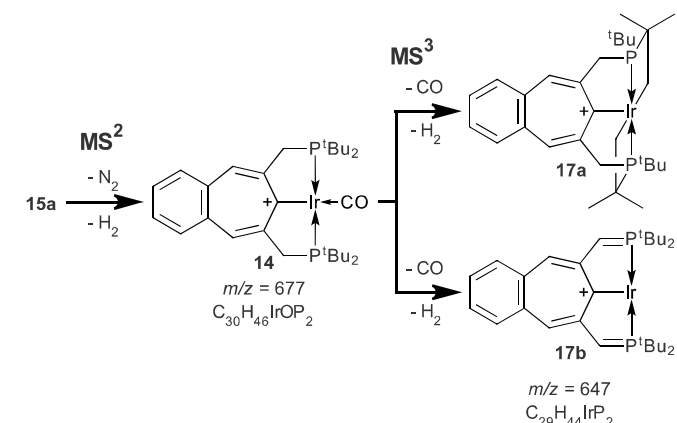
Figure 9: ESI mass spectra of **6a**: a) with routine infusion set-up, b) with the improved infusion set-up.

The application of the improved infusion set-up (Figure S2) led to a mass spectrum of **6a** which exclusively displays the m/z 707 corresponding to complex **15a** while m/z 677 as well as m/z 693 and therefore **14** and the oxo complex **16**, respectively are missing (Figure 9b). Complex **15a** can be rationalised as the trapping product of **10** with nitrogen. The missing signals of the “decomposition” product **14** or of the reaction product **16** verifies m/z 707 (**10**) as the initially formed ion under inert conditions (improved infusion set-up).

TANDEM-MS EXPERIMENTS AND FAB FRAGMENTATION

The following schemes show the fragmentation pathway of **6a** as derived from MS^n experiments and the FAB mass spectrum (Figure 4). The sum formula in Scheme 8 and 9 are obtained from high-resolution mass spectra using ESI in-source fragmentation experiments. The tandem MS experiments were

performed with the routine set-up for ESI infusion and the entire isotope pattern of the respective m/z was collected in the ion-trap and the fragmentation induced. There is no clean fragment ion signal observed for the collision induced dissociation (CID) of the ions with m/z 693 (**16**). The first CID of the nitrogen adduct complex **15a** (m/z 707) forms the Ir(I) compound **14** (m/z 677) by elimination of dinitrogen and dihydrogen (Scheme 8).



Scheme 8

This MS^2 result verifies the previous assumption of the fragmentation derived from the spectra with different capillary exit potentials (in-source fragmentation). Starting from the dinitrogen complex **15a**, the reaction to **14** is by 37.3 kJ/mol endergonic (Figure 8). A further CID step is accompanied by the formal removal of carbon monoxide and molecular hydrogen resulting in the isomeric complexes **17a** or **17b** (m/z 647) (Scheme 8).

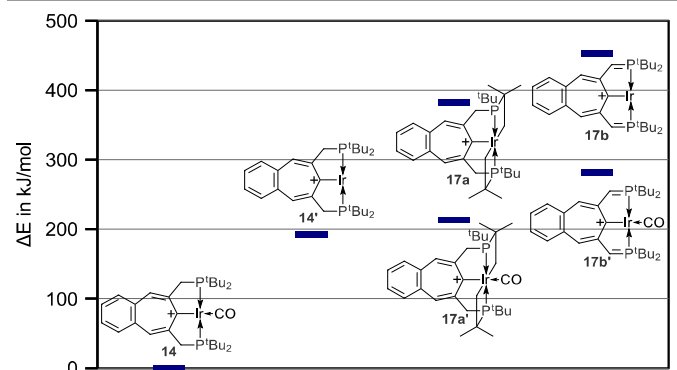
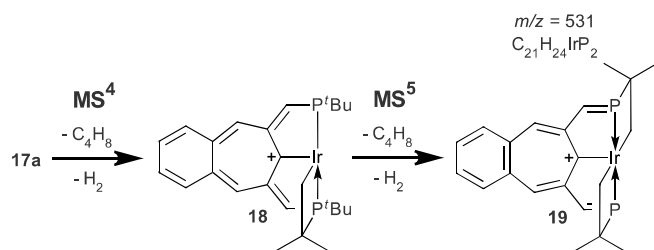


Figure 10: DFT energies (relative to the energy of **14**) of the species in Scheme 8 including some intermediates.

The Ir(III) complex **17a** displays two cyclometallated *tert*-butyl groups and an aromatic backbone. In solution chemistry, examples of this type of intra-molecular activation of sp^2 and sp^3 C-H bonds in rhodium,⁴² iridium^{43–47} and ruthenium^{48,49} complexes are well known. In **17b** the positive charge is also delocalised in the aromatic BCHT backbone while the Ir(I) centre is coordinated by phosphanylidene moieties. There are isolated and characterised examples of transition metal

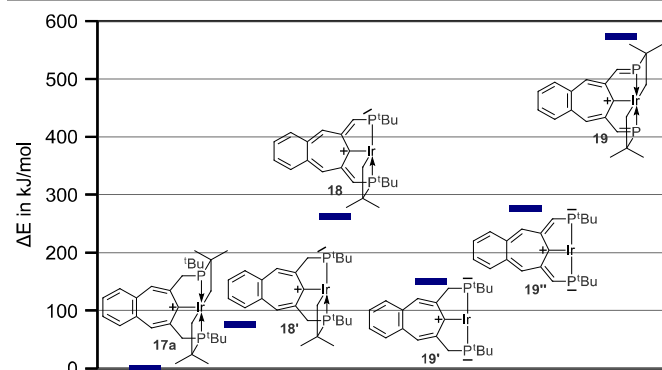
phosphanylidene complexes in solution chemistry.^{50–53} The contribution of some non-aromatic resonance structures in **17b** destabilises this structure compared to the isomeric compound **17a** by 70.0 kJ/mol (Figure 10). It is assumed that initially CO is released to create an active $14e^-$ Ir(I) species (**14'** in Figure 10) which is 192.5 kJ/mol higher in energy than **14** and not observed in the mass spectra. Subsequently, there are two possibilities to transfer two hydrogen atoms intra-molecularly from the ligand backbone to the metal centre in **14'**. This is the essential condition for a reductive elimination of a dihydrogen molecule. First consecutive cyclometallations of two *tert*-butyl groups consume 190.2 kJ/mol and finally generating isomer **17a**. Second the concerted shifts of two γ -hydrogen atoms from the methylene bridges to the metal centre forming complex **17b**, which requires 260.2 kJ/mol. Furthermore, in Figure 10 the carbonyl complexes **17a'** and **17b'** are shown which could be formed by alternative pathways with initial cyclometallation or γ -hydrogen shifts. Although, the complexes **17a** and **17b** are higher in energy (168.9 kJ/mol and 171.4 kJ/mol) than their carbonyl counterparts (**17a'** and **17b'**), the formation of the $14e^-$ Ir(I) complex **14'** is thermodynamically preferred by 21.3 kJ/mol and 88.8 kJ/mol as compared to **17a'** and **17b'**. This justifies the assumption of the initial carbon monoxide emission and the subsequent removal of dihydrogen.



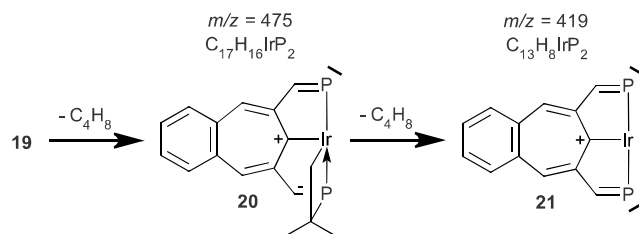
Scheme 9

A further CID step applied on complex **17a** (Scheme 9) generates a signal at m/z 589 which is consistent with the result of *iso*-butene and dihydrogen elimination. In Scheme 9 the structures from the iridium complexes **18** and **19** are shown which are formed by formal 2+2 cycloeliminations and H_2 elimination. The asymmetric structure of compound **18** displays one metal coordinated *tert*-butyl phosphanylidene arm and one residual cyclometallated *tert*-butyl group. In this structure the BCHT backbone is slightly twisted, mainly in the CHT ring, thereby losing aromaticity. Due to decreasing intensities in MS^n spectra the last observable fragment ion in ESI-ion-trap- MS is m/z 531 which is assigned to structure **19** (Scheme 9). The remaining *tert*-butyl groups in compound **19** were activated forming two four membered rings linked *via* the iridium atom and molecular hydrogen. Energetically, the release of *iso*-butene from **17a** is an endergonic reaction (75.8 kJ/mol) *via* a formal 2+2 cycloelimination and hence the formation of a formal iridium phosphide single bond according to **18'** in Figure 11. Although, the subsequent emission of a further equivalent of *iso*-butene forming **19'** is 112.5 kJ/mol less endergonic than the removal of dihydrogen leading to **18**, the

mass experiment confirms the exclusive generation of **18** (186.0 kJ/mol relative to **18'**).

Figure 11: DFT energies (relative to the energy of **17a**) of the species in Scheme 9 including some intermediates.

Therefore the activation barrier for *iso*-butene cycloelimination seems to be significantly higher than the barrier for γ -hydrogen shifts from the methylene bridges to the metal and subsequent reductive elimination of H_2 . The cycloelimination of *iso*-butene from **18** affording the bis-*tert*-butylphosphanylidene complex **19''** is only weakly endergonic (14.0 kJ/mol), while the consecutive cyclometallation of the *tert*-butyl groups and the elimination of dihydrogen which yield **19** are in sum 297.9 kJ/mol higher in energy than **18**. Additionally, to the m/z signals 647, 589 and 531 from the ESI MS^n experiments the FAB mass spectrum (Figure 3) displays two further fragment ions with m/z 475 and 419. The consecutive elimination of two neutral *iso*-butene fragments with m/z 56 explains the observed fragment masses and allows their attribution to the structures **20** and **21** (Scheme 10). Both structures are available from formal 2+2 cycloeliminations yielding the Ir(III) complexes.



Scheme 10

The shown resonance structure of compound **20** contains an Ir(III) centre with an almost planar carbo-cyclic backbone, one *tert*-butyl phosphanylidene arm with cyclometallated *tert*-butyl group and one coordinated phosphanylidene moiety. In complex **21** the remaining cyclometallated *tert*-butyl group was emitted as an *iso*-butene molecule forming a C_{2v} symmetric iridium complex with two coordinated phosphanylidene arms and the central carbon metal bond. The iridium atom is located above the plane formed by the phosphorus atoms and the central carbon atom and seems to become additionally stabilised by interacting with the carbon phosphorus double bond (see Table S5, supplementary information).

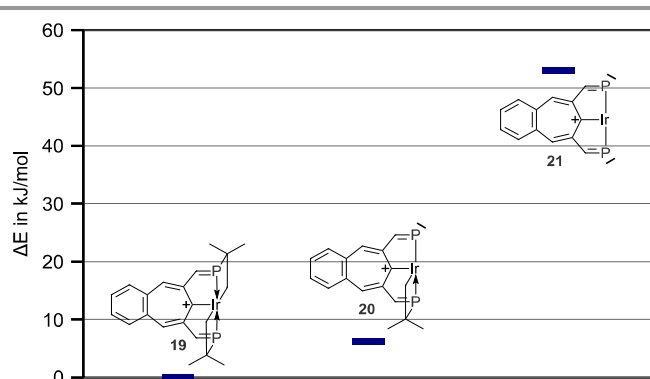
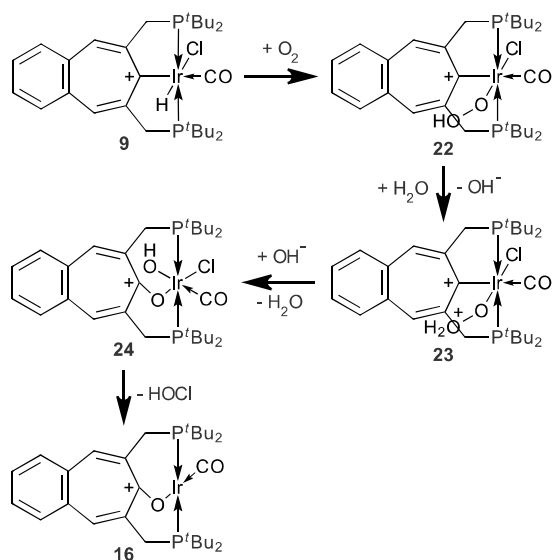


Figure 12: DFT energies (relative to the energy of **26**) of the species in Scheme 11.

Thermodynamically, the cycloelimination of one *iso*-butene molecule from **19** is with 6.2 kJ/mol only slightly endergonic. On the other hand the elimination of the *iso*-butene molecule from **20** forming the bis-phoshanylidenide complex **21** is a comparatively energy consuming process (46.9 kJ/mol).

Synthetic approach to the BCHT iridium oxo-complex **16**

The formation of the cationic oxo-complex **16** (Scheme 11) was first proposed analysing the different mass spectra of **6a** (Scheme 7 and Figure 8). Previously the corresponding CHT oxo-complex was prepared using atmospheric air and characterised by NMR spectroscopy as well as single crystal XRD.³⁹ This procedure was modified and applied to the cationic BCHT complex **9** to achieve the structural verification and characterisation.



Scheme 11

Therefore the hydrido chloro complex **6a** dissolved in DCM-*d*₂ is treated with stoichiometric amounts of triphenylcarbenium tetrafluoroborate in an NMR-tube and the resulting crude mixture is saturated with pure oxygen. Due to the similarity of the ³¹P chemical shifts of the CHT and BCHT complexes the chemical shift of **16** is also expected to be close to the chemical

shift of the analogous cycloheptatriene oxo-complex (δ_P 86.9).³⁹ The reaction of **9** with pure oxygen was monitored over a period of 76 days (see figure S3, supplementary information). Thereby the cationic hydrido chloro complex **9** at δ_P 60.5 is slowly transformed into two symmetric compounds resonating at δ_P 77.9 and 42.5, respectively, in roughly equal amounts (see Figure S3, in the supplementary informations). The corresponding ¹H NMR spectra show a hydride signal of the residual cationic complex **9** but there are no further hydride resonances observable. Furthermore in the product the numbers of signals in the low-field region are identical and their principal coupling patterns are rather similar as compared to **9**. The ¹H signals of the aromatic backbone and of the bridging methylene groups of the compound associated with δ_P 77.9 are shifted to higher fields while the same signals of the complex linked to δ_P 42.5 are shifted to lower fields as compared to the cationic species **9**. The chemical shift of δ_P 77.9 and the corresponding ¹H NMR data are comparable to those of the CHT oxo complex³⁹ and are thus assigned to the BCHT oxo complex **16** (Scheme 11). Compound **9** can be attacked by singlet oxygen at the metal carbon, the metal hydrogen and the metal chlorine bond, respectively. Thermodynamically, the addition of O₂ to the Ir-C bond and the additional hydride shift to the terminal oxygen is formed exothermic (-111.6 kJ/mol, **22b** in Figure S4 and Table S6 of the supplementary informations). The insertion of singlet oxygen into the Ir-Cl bond is slightly endothermic (2.8 kJ/mol, **22a** in Figure S4 and Table S6) and the insertion into the Ir-H bond forms the most stable hydro-peroxide species **22** (-168.7 kJ/mol). Assuming traces of water present in the reaction medium the terminal hydroxy group of the hydro-peroxide might become protonated. The resulting bis-cationic complex **23** eliminates the water molecule simultaneously forming the oxo-bridge and an iridium localised cation. This might be intercepted by a hydroxide ion or a water molecule yielding the oxo-bridged mono-cationic hydroxo complex **24** which presents a hexa-coordinated metal centre with a *cis*-arrangement of the hydroxide and chloride ligand. Finally the reductive elimination of hypochlorous acid forms the Ir(I) oxo-complex **16**.

Experimental section

General informations

All syntheses were carried out with standard Schlenk technique under an atmosphere of Argon (99.999 % purity) unless noted otherwise.

The solvents (reagent grade) were obtained from varying chemical distributors. THF in reagentplus quality was purchased from Sigma-Aldrich and *n*-pentane 99+ % extrapure from Acros Organics. Solvents were dried according to literature methods and distilled under Argon. Diethyl ether and THF were dried over sodium/benzophenone, ethanol over sodium, dichloromethane over calcium hydride, *n*-pentane over sodium hydride and acetone over sicapent (P₂O₅). The dry solvents were stored under Argon in Schlenk flasks with activated molecular sieve (3 Å or 4 Å).

Deuterated solvents were obtained from Deutero GmbH or from Eurisotop (no less than 99.8% deuteration), transferred to Schlenk flasks with activated molecular sieves, degassed by three freeze-pump-thaw cycles and used without further purification.

Tetrabromomethane, phosphorus tribromide, pyridine, tritylium tetrafluoroborate, hydrobromic acetic acid solution, trimethylsilyl trifluoromethanesulfonate, tetrabutylammonium bromide, triphenylphosphine, and boron trifluoride diethyl etherate were purchased from Sigma Aldrich Chemical Company. Di-tert-butylphosphine was obtained from ABCR Chemical Company and $(\text{CO})_3\text{IrCl}$ from Strem Chemicals. The commercially available reagents were used without further purification unless otherwise noted.

Analytical methods

All NMR spectra were recorded at a temperature of 299K on the following spectrometers: (i) Bruker DRX 250 MHz spectrometer equipped with a 5mm BBO probe with automatic tuning and matching: ^1H : 250.13 MHz; ^{11}B : 80.25 MHz; ^{13}C : 62.90 MHz; ^{31}P : 101.25 MHz. (ii) Bruker Avance II 400 MHz spectrometer equipped with a 5mm QNP probe including Z-gradient: ^1H : 400.13 MHz; ^{13}C : 100.61 MHz; ^{19}F : 376.50 MHz; ^{31}P : 161.98 MHz. (iii) Bruker Avance II+ 500 MHz spectrometer with a 5mm TBO probe including Z-gradient: ^1H : 500.13 MHz; ^{11}B : 160.46 MHz; ^{13}C : 125.76 MHz; ^{31}P : 202.46 MHz. ^1H NMR spectra were referenced to the residual signals of the deuterated solvent relative to 1 % TMS in CDCl_3 . ^{13}C NMR spectra were referenced to the signal of deuterated solvent relative to 1 % TMS in CDCl_3 . ^{11}B , ^{19}F and ^{31}P NMR spectra were indirectly referenced *via* the deuterium (lock) signal of the solvent to 1 % TMS in CDCl_3 using the respective reference frequencies ratio $\bar{\nu}_{X,Ref}$ as recommended.⁵⁴ The description of the multiplet patterns in the analytic part is especially for the compounds containing phosphorus rather difficult due to the most often very complicated spin systems. Different coupling paths of chemically equivalent nuclei in these compounds are the reason for magnetic in-equivalence leading to higher order spin systems (N-line spectra). If higher order multiplets are observed in the spectra this is indicated in the analytic data as virtual multiplets (vd, vt, vdd, etc.). In case of assignable N-lines their distance is given in the analytic data. If the N-lines could not be assigned the coupling constants are determined as in a zero-order multiplet but without the declaration of the number of the bonds linking the coupled nuclei.

ESI mass spectra were recorded on a Bruker Daltonics Esquire3000+ mass spectrometer. This instrument uses an ion trap as *m/z* filter and is additionally able to perform experiments with collected ions. To catch ions in the ion trap they have to get rid of their kinetic energy by a collision gas (bath gas, He) to become stored at the bottom of a potential trough. The application of an additional radio frequency potential allows the successive ejection of ions with different *m/z* from the ion trap and therefore the scanning of the accessible *m/z* range. Furthermore, ions with a selected *m/z* can be isolated in the ion

trap and fragmented by excitation with a low voltage (0.6 to 1.2 V) radio frequency potential (too less to become ejected). The selected ions become accelerated in the trap and the higher energy collisions with the bath gas (He) induces the fragmentation of the isolated ion. This process is called collision induced dissociation (CID). Afterwards, these new fragment ions can also be isolated and fragmented. These types of experiments are referred to as tandem mass spectrometry or MS^n experiments. The Bruker Daltonics Esquire3000+ allows the subsequent isolation and fragmentation in up to ten steps. Typically ESI mass spectra of organometallic compounds were obtained by direct infusion of a 1-20 $\mu\text{mol/L}$ DCM solution with a syringe pump at a flow rate of 10-20 $\mu\text{L/min}$. The sample solutions were prepared with dry solvents in an HPLC vial equipped with a PTFE septum. Prior to the injection a gas-tight 0.5 mL or 1 mL Hamilton syringe with a blunt needle point was flushed five times with argon. The sample solution was drawn up, the filled syringe was placed in a syringe pump and connected *via* a transfer capillary (PEEK or PTFE) to the spray chamber (also see ESI). For HR-ESI mass spectra a Bruker Daltonics 4.7 T APEX II FT-ICR instrument was used with direct infusion of a $\leq 1 \mu\text{mol/L}$ sample solution containing methanol. As internal mass reference an adequate poly(ethylene glycol) was applied. In this case the sample preparation and the infusion process were done in air. Fast atom bombardment (FAB) mass spectra were measured on a Finnigan MAT TSQ 70 mass analyser using 3-nitrobenzyl-alcohol as matrix. Elemental analyses were performed using a Vario EL analyser from Elemental Company. BCHT dialdehyde (**1**)³⁷ and di-tert-butylphosphine^{55,56} were prepared according to literature procedures. Melting points (uncorrected) were determined with a BÜCHI Melting Point B-540 device.

Syntheses

BCHT DIOL (**2**)

To a suspension of **1** (7.35 g, 37.1 mmol) in ethanol (450 ml) a mixture of sodium borohydride (2.95 g, 77.9 mmol) and Na_2CO_3 (7.12 g, 74.1 mmol) was added in portions. After 6 h stirring at room temperature the solids were removed via filtration (P3) and the volatile parts of the filtrate were removed *in vacuo*. The yellow residue was dissolved in ethyl acetate (550 ml), flashed over a short silica gel column (P3) and the solvent was removed under vacuum. The resulting pale yellow solid was dissolved in chloroform and extracted with saturated NaHCO_3 solution and water. The organic layer was dried over Na_2SO_4 . Removal of the solvent under vacuum afforded a pale yellow solid. Yield: 73 %.

^1H NMR (400.13 MHz, CDCl_3): 1.87 (s, 2H, CH_2OH); 2.56 (s, 2H, CH_2CHT); 4.32 (s, 4H, CH_2OH); 6.58 (s, 2H, CH_{CHT}); 7.23-7.33 (m, 4H, $\text{CH}_{\text{Benzo-o,m-CHT}}$). $^{13}\text{C}\{^1\text{H}\}$ NMR (100.13 MHz, CDCl_3): 29.1 (CH_2CHT); 67.4 (CH_2OH); 125.5 (CH_{CHT}); 126.1 ($\text{CH}_{\text{Benzo-m-CHT}}$); 130.1 ($\text{CH}_{\text{Benzo-o-CHT}}$); 135.9 (C_{Benzo}); 141.2 (C_{CHT}). Elemental Analysis: Found: C, 77.22; H, 6.50 %. Calc. for $\text{C}_{13}\text{H}_{14}\text{O}_2$: C, 77.20; H, 6.98 %. MS (EI) *m/z*: 202.1, $[\text{M}]^+$; 184.2, $[\text{M}-\text{H}_2\text{O}]^+$. Mp: 131 °C.

BCHT DIBROMIDE (**3**) (SEE SUPPLEMENTAL INFORMATION)

A mixture of **2** (2.00 g, 9.88 mmol) and pyridine (0.475 g, 6.00 mmol) was dissolved in diethyl ether (20 ml) and cooled to 0 °C. Phosphorus tribromide (3.25 g; 12.0 mmol) was added drop wise over a period of 30 min. The cool bath was removed after 30 min stirring and the yellow suspension was heated to 40 °C for 6 h. The reaction was quenched with saturated NaHCO₃ solution until the pH was around 6-7. The aqueous layer was extracted with diethyl ether (100 ml). The combined organic layers were dried over Na₂SO₄ and evaporated to dryness. The crude product was purified by column chromatography yielding an off-white solid (SiO₂, cyclohexane:DCM = 3:1). Yield: 88 %.

¹H NMR (400.13 MHz, CDCl₃): 2.56 (s, 2H, CH₂CHT); 4.20 (s, 4H, CH₂Br); 6.63 (s, 2H, CH_{CHT}); 7.19 (m, 4H, CH_{Benzo-o,m-CHT}). ¹³C{¹H} NMR (100.13 MHz, CDCl₃): 31.9 (CH₂CHT); 39.0 (CH₂Br); 126.9 (CH_{Benzo-m-CHT}); 129.4 (CH_{CHT}); 130.5 (CH_{Benzo-o-CHT}); 135.6 (C_{CHT}); 137.2 (C_{Benzo}). Elemental analysis: Found: C, 47.25; H, 3.40 %. Calc. for C₁₃H₁₂Br₂: C, 47.60; H, 3.69 %. MS (EI) *m/z*: 329.9, [M]⁺; 249.0, [M-Br]⁺; 168.1, [M-2Br]⁺.

BCHT BIS-(DI-TERT-BUTYLPHOSPHONIUM BROMIDE) (4)

To a solution of **3** (1.80 g, 5.49 mmol) in acetone (35 ml) di-*tert*-butylphosphane (1.60 g, 10.97 mmol) was added drop wise over a period of 30 min. The suspension was heated to 60 °C for 4 h. The precipitate was removed via filtration, washed with acetone (30 ml) and dried under vacuum. Yield: >95 %.

³¹P{¹H} NMR (161.98 MHz, D₂O): 35.9 (t, ¹J_{PD} = 65.37 Hz). ¹H NMR (400.13 MHz, D₂O): 1.59 (d, ³J_{PH} = 16.95 Hz, 36H, C(CH₃)₃), 2.73 (bs, 2H, CH₂CHT), 3.71 (d, ²J_{PH} = 13.65 Hz, 4H, CH₂P), 6.95 (d, ⁴J_{PH} = 3.19 Hz, 2H, CH_{CHT}), 7.44 (m, 4H, CH_{Benzo-o,m-CHT}). ¹³C{¹H} NMR (100.13 MHz, D₂O): 134.9 (s, C_{CHT}); 132.7 (s, CH_{CHT}); 132.6 (s, C_{Benzo}); 130.0 (s, CH_{Benzo}); 127.6 (s, CH_{Benzo}); 34.9 (s, CH₂CHT); 33.1 (d, A₂X, ¹J_{PC} = 33.17 Hz, C(CH₃)₃); 26.8 (s, C(CH₃)₃); 24.8 (d, AX, ¹J_{PC} = 38.15 Hz, CH₂P). Elemental analysis: Found: C, 55.88; H, 7.69 %. Calc. for C₂₉H₅₀P₂Br₂: C, 56.14; H, 8.12 %.

BCHT BIS-(DI-TERT-BUTYLPHOSPHANE) (5)

The phosphonium salt (**4**) was dissolved in degassed water (20 ml) and overlaid with diethyl ether. The salt is then hydrolysed with a solution of potassium *tert*-butanolate (1.23 g, 10.97 mmol) in water (5 ml) and **5** extracted with diethyl ether. The organic layer was evaporated to dryness yielding a pale yellow solid. Yield: >95 %.

³¹P{¹H} NMR (202.46 MHz, DCM-d₂): 16.1 (s). ¹H NMR (500.13 MHz, DCM-d₂): 7.15 (2H, m, CH_{Benzo-o-CHT}); 7.01 (2H, m, CH_{Benzo-m-CHT}); 6.45 (2H, br s, CH_{CHT}); 2.81 (4H, d, A₂X, ²J_{PH} = 4.30 Hz, CH₂P); 2.76 (2H, t, A₂X₂, ⁴J_{PH} = 1.30 Hz, CH₂CHT); 1.19 (36H, d, A₁₈X, ³J_{PH} = 10.65 Hz, C(CH₃)₃). ¹³C{¹H} NMR (125.76 MHz, DCM-d₂): 143.5 (vdd, AXX', ¹J_{PC} = 11.54 Hz, ¹J_{PC} = 0.88 Hz, C_{CHT}); 137.7 (vt, AXX', N = [⁴J_{PC}+⁵J_{PC}] = 2.39 Hz, C_{Benzo}); 130.1 (vd, AXX', ¹J_{PC} = 1.26 Hz, CH_{Benzo-o-CHT}); 127.1 (vd, AXX', ¹J_{PC} = 7.95 Hz, CH_{CHT}); 125.7 (s, CH_{Benzo-m-CHT}); 36.2 (t, A₂X₂, ³J_{PC} = 9.43 Hz, CH₂CHT); 34.5 (vdd, AXX', ¹J_{PC} = 24.57 Hz, ¹J_{PC} = 4.18 Hz, CH₂P); 32.6 (d, A₂X, ¹J_{PC} = 23.94 Hz, C(CH₃)₃); 30.5 (d, A₆X, ²J_{PC} = 13.46 Hz, C(CH₃)₃). MS (EI) *m/z*: 458.3, [M]⁺.

BCHT PCPIrHCLCO (6a-c)

General Procedure: Ligand **5** (101 mg, 220 μmol) was mixed with degassed Ir(CO)₃Cl (70.4 mg, 226 μmol) in solid state. The reaction was started by the addition of 2 mL of THF. The resulting yellow to brown suspension was vigorously stirred at temperatures between 40 °C and 45 °C without pressure equilibration. At temperatures higher than 50 °C the products of the isomerisation process were also formed as side products. The overall reaction times vary significantly between 14 h and 30 h which is the reason for the monitoring of the reaction *via* ³¹P{¹H} NMR. If necessary degassed Ir(CO)₃Cl was added stepwise until more than 90 % (based on the integration of the ligand signal in the ³¹P{¹H} spectra) conversion was achieved. Subsequently, the solid components of the suspension were separated by centrifugation. The dark solid was washed three times with 2 mL of THF. From the combined yellow liquid phases containing the product the solvent was removed by vacuum distillation. A yellow solid was obtained in yields exceeding 90 % containing mainly **6a** and occasionally **6b** and **6c**. At higher reaction temperatures the colour of the reaction mixture turns to orange which is indicative for additional backbone isomerisations. We were not able to isolate any pure product from these types of mixtures.

IR: (KBr pellets) $\tilde{\nu}(\text{CO}) = 2000 \text{ cm}^{-1}$, $\tilde{\nu}(\text{IrH}) = 2280 \text{ cm}^{-1}$; (CCl₄ solution) $\tilde{\nu}(\text{CO}) = 2009 \text{ cm}^{-1}$, $\tilde{\nu}(\text{IrH}) = 2258 \text{ cm}^{-1}$. HR-MS (ESI) *m/z*: calc. 707.28656 for ¹²C₃₀ ¹H₄₈ ¹⁹³Ir ¹⁴N₂ ¹⁶O ³¹P₂; exp. 707.28862 [M-Cl+N₂]⁺. Elemental analysis: Found: C 50.43, H 7.05 %. Calc. for C₃₀H₄₈IrOP₂Cl: C 50.44 %, H 6.77 %.

Isomer 6a:

³¹P{¹H} NMR (161.98 MHz, DCM-d₂): 49.0 (s). ¹H NMR (400.13 MHz, DCM-d₂): 7.119 (m, 2H, CH_{Benzo-o-CHT}); 7.124 (m, 2H, CH_{Benzo-m-CHT}); 6.68 (m, 2H, CH_{CHT}); 3.68 (m, 1H, CH_{CHT-Ir}); 3.52 (m, 2H, CHHP); 3.06 (m, 2H, CHHP); 1.47 (vt, [A₉X]₂, N = [³J_{PH}+⁵J_{PH}] = 14.08 Hz, 18H, C(CH₃)₃); 1.36 (vt, [A₉X]₂, N = [³J_{PH}+⁵J_{PH}] = 13.16 Hz, 18H, C(CH₃)₃); -18.85 (t, AX₂, ²J_{PH} = 14.29 Hz, 1H, IrH). ¹³C{¹H} NMR (100.61 MHz, DCM-d₂): 177.7 (t, AX₂, ²J_{PC} = 7.10 Hz, IrCO); 154.5 (AXX', N = [²J_{PC}+⁴J_{PC}] = 13.62 Hz, C_{CHT}); 137.6 (s, C_{Benzo}); 129.9 (s, CH_{Benzo-m-CHT}); 125.7 (s, CH_{Benzo-o-CHT}); 122.7 (AXX', N = [³J_{PC}+⁵J_{PC}] = 14.99 Hz, CH_{CHT}); 45.7 (AXX', N = [¹J_{PC}+³J_{PC}] = 32.92 Hz, CH₂P); 42.8 (t, AX₂, ²J_{PC} = 2.72 Hz, CH_{CHT-Ir}); 39.1 (AXX', N = [¹J_{PC}+³J_{PC}] = 16.57 Hz, C(CH₃)₃); 36.0 (AXX', N = [¹J_{PC}+³J_{PC}] = 26.56 Hz, C(CH₃)₃); 31.2 (AXX', N = [²J_{PC}+⁴J_{PC}] = 3.79 Hz, C(CH₃)₃); 29.5 (AXX', N = [²J_{PC}+⁴J_{PC}] = 4.20 Hz, C(CH₃)₃).

Isomer 6b:

³¹P{¹H} NMR (161.98 MHz, DCM-d₂): 46.0 (s). ¹H NMR (400.13 MHz, DCM-d₂): 6.85 (m, 3H, CH_{Benzo-o-CHT}); 6.63 (m, 2H, CH_{Benzo-m-CHT}); 5.49 (m, 2H, CH_{CHT}); 3.81 (m, 1H, CH_{CHT-Ir}); 2.79 (m, [ABX]₂, ²J_{HH} = 14.52 Hz, N = [²J_{PH}+⁴J_{PH}] = 6.56 Hz, 2H, CHHP); 2.15 (m, [ABX]₂, 2H, CHHP); 1.54 (vt, [A₉X]₂, N = [³J_{PH}+⁵J_{PH}] = 14.16 Hz, 18H, C(CH₃)₃); 1.32 (vt, [A₉X]₂, N = [³J_{PH}+⁵J_{PH}] = 13.24 Hz, 18H, C(CH₃)₃); -17.77 (t, AX₂, ²J_{PH} = 12.76 Hz, 1H, IrH). ¹³C{¹H} NMR (100.61 MHz, DCM-d₂): 146.3 (AXX', N = [²J_{PC}+⁴J_{PC}] = 7.15 Hz, C_{CHT}); 136.2 (s, C_{Benzo}); 131.2 (s,

CH_{Benzo-m-CHT}); 126.9 (s, CH_{Benzo-o-CHT}); 126.3 (AXX', N = $^2J_{PC} + ^5J_{PC}$ = 14.65 Hz, CH_{CHT}); 39.7 (AXX', N = $^1J_{PC} + ^3J_{PC}$ = 17.26 Hz, C(CH₃)₃); 37.8 (s, CH_{CHT-Ir}); 37.1 (AXX', N = $^1J_{PC} + ^3J_{PC}$ = 24.29 Hz, CH₂P); 36.4 (AXX', N = $^1J_{PC} + ^3J_{PC}$ = 24.52 Hz, C(CH₃)₃); 31.3 (AXX', N = $^2J_{PC} + ^4J_{PC}$ = 3.97 Hz, C(CH₃)₃); 30.1 (AXX', N = $^2J_{PC} + ^4J_{PC}$ = 5.22 Hz, C(CH₃)₃); carbonyl not observed.

Isomer 6c:

$^{31}P\{^1H\}$ NMR (161.98 MHz, acetone-*d*₆): 61.5 (s). 1H NMR (400.13 MHz, DCM-*d*₂): -10.09 (1H, t, AX₂, $^2J_{PH}$ = 14.54 Hz, IrH). Since 6c is the isomer with the smallest amount in the mixture and due to overlapping signals in 1H and $^{13}C\{^1H\}$ NMR spectra the 1H and ^{13}C chemical shifts could not be determined reliably.

BCHT PCPIrHClCO BF₄ (9)

General Procedure: In a J. Young NMR-Tube a solution of 6 (8.58 mg, 12.0 μmol) in 0.2 mL of DCM-*d*₂ was prepared. A solution of degassed Ph₃CBF₄ (4.23 mg, 12.8 μmol) in 0.2 mL of DCM-*d*₂ was prepared separately. The Ph₃CBF₄ solution was added speedily to the solution in the J. Young tube, thereby the colour of the reaction mixture turns instantly from yellow to red-orange. The $^{31}P\{^1H\}$ spectrum reveals the nearly quantitative formation of the cationic complex 9. The red crystalline product could be obtained by adding *n*-pentane to the red DCM solution.

$^{31}P\{^1H\}$ NMR (161.98 MHz, DCM-*d*₂): 59.6 (s). $^{19}F\{^1H\}$ NMR (376.50 MHz, DCM-*d*₂): -150.6 (br. s, BF₄⁻). $^{11}B\{^1H\}$ NMR (80.25 MHz, DCM-*d*₂): 0.8 (br. s, BF₄⁻). 1H NMR (400.13 MHz, DCM-*d*₂): 9.25 (s, 2H, CH_{CHT}); 8.44 (m, 2H, CH_{Benzo-o-CHT}); 8.18 (m, 2H, CH_{Benzo-m-CHT}); 4.89 (m, [ABX]₂, $^2J_{HH}$ = 16.73 Hz, N = $^2J_{PH} + ^4J_{PH}$ = 7.68 Hz, 2H, CHHP); 4.32 (m, [ABX]₂, $^2J_{HH}$ = 16.73 Hz, N = $^2J_{PH} + ^4J_{PH}$ = 8.03 Hz, 2H, CHHP); 1.51 (vt, [A₉X]₂, N = $^3J_{PH} + ^5J_{PH}$ = 14.78 Hz, 18H, C(CH₃)₃); 1.32 (vt, [A₉X]₂, N = $^3J_{PH} + ^5J_{PH}$ = 14.15 Hz, 18H, C(CH₃)₃); -16.91 (t, AX₂, $^2J_{PH}$ = 12.53 Hz, 1H, IrH). $^{13}C\{^1H\}$ NMR (100.61 MHz, DCM-*d*₂): 228.2 (t, AX₂, $^2J_{PC}$ = 2.56 Hz, C_{CHT-Ir}); 176.3 (t, AX₂, $^2J_{PC}$ = 7.21 Hz, IrCO); 165.6 (AXX', N = $^2J_{PC} + ^4J_{PC}$ = 13.62 Hz, C_{CHT}); 146.2 (AXX', N = $^2J_{PC} + ^4J_{PC}$ = 13.74 Hz, CH_{CHT}); 141.1 (s, C_{Benzo}); 136.7 (s, CH_{Benzo-m-CHT}); 136.2 (s, CH_{Benzo-o-CHT}); 46.1 (AXX', N = $^1J_{PC} + ^3J_{PC}$ = 27.48 Hz, CH₂P); 39.6 (AXX', N = $^1J_{PC} + ^3J_{PC}$ = 21.23 Hz, C(CH₃)₃); 37.6 (AXX', N = $^1J_{PC} + ^3J_{PC}$ = 26.79 Hz, C(CH₃)₃); 30.2 (s, C(CH₃)₃).

REACTION OF BCHT PCPIrHClCO BF₄ (16) WITH O₂

In a J. Young NMR tube a solution of 9 in DCM-*d*₂ was prepared as described in the former paragraph and used without separating the simultaneously formed triphenylmethane. This solution was degassed by three pump-freeze-thaw cycles and consecutively the solution is saturated with oxygen. Over a period of 2.5 months this sample was stored at room temperature, without exclusion of daylight and was vigorously shaken from time to time.

$^{31}P\{^1H\}$ NMR (202.46 MHz, DCM-*d*): 76.9 (s). 1H NMR (500.13 MHz, DCM-*d*₂): 8.59 (m, 2H, CH_{CHT}); 8.16 (m, 2H, CH_{Benzo-m-CHT}); 7.98 (s, 2H, CH_{Benzo-o-CHT}); 3.68 (m, [ABX]₂, $^2J_{HH}$ = 14.23 Hz, N = $^2J_{PH} + ^4J_{PH}$ = 9.50 Hz, 2H, CHHP); 3.55

(m, [ABX]₂, $^2J_{HH}$ = 14.23 Hz, N = $^2J_{PH} + ^4J_{PH}$ = 6.58 Hz, 2H, CHHP); 1.57 (vt, [A₉X]₂, N = $^3J_{PH} + ^5J_{PH}$ = 14.44 Hz, 18H, C(CH₃)₃); 1.32 (vt, [A₉X]₂, N = $^3J_{PH} + ^5J_{PH}$ = 14.44 Hz, 18H, C(CH₃)₃).

Computational details

All calculations were performed with Jaguar, the ab initio quantum mechanic package from Schrödinger LLC.⁵⁷ Maestro⁵⁸ was used as graphical user interface to import or modify the input structures and generate the input files for Jaguar. Furthermore the Jaguar output structures, molecular orbitals and vibrational data were analysed with Maestro. Initially, an Intel Pentium4 3.2 GHz (32bit) and thereafter an Intel Core2Duo E8400 (64bit) personal computer was used as hardware platform which run under OpenSuSE Linux.

Unless otherwise mentioned the B3LYP hybrid functional^{59,60} was used with the Los Alamos LACVP* valence double zeta basis set⁶¹ for all DFT calculations. LACVP is an Effective Core Potential (ECP) basis set treating the core electrons of heavier elements than Argon with a relativistic effective potential while the electrons of the valence shell (e.g. Iridium: 5s5p6s5d6p) are calculated explicitly. Elements lighter than Argon use the split valence 6-31G* basis set.⁶²⁻⁶⁶ Furthermore the LACVP* basis set is optimised for pseudospectral⁶⁷ calculations. Usually for all calculations the grid density for numerical integration and the accuracy level for integral cut-offs was set to "medium" and "quick" respectively. The default thresholds for the SCF convergence were used.

Generally the input structures for geometry optimisations were obtained from modified or unmodified crystal structures or by modification of a previously calculated crystal structure. The default thresholds for the convergence of the geometry optimisation were used. There were no symmetry settings or structural constraints applied nor any *tert*-butyl group substitution prior to the calculations. If geometry convergence could not be achieved with the default settings, the grid density was increased to "maximum" and the pseudo-spectral calculation was turned off by setting the accuracy level to "fully analytic". Regularly the vibrational frequencies were calculated from the Hessian of the final geometry optimisation step to verify the minimum structure. All optimised structures are depicted in Table S5 in the supplementary informations.

Conclusions

The novel benzo annulated cycloheptatriene (BCHT) PCP pincer ligand 5 was synthesised in a multi-step synthesis in high overall yields. The synthetic accessibility of this new sp³-pincer ligand is a significant simplification as compared to the cycloheptatriene based ligand. Also the coordination chemistry of this ligand with iridium is comparable to its previous counterpart. The tendency for backbone isomerisations is also observed for the BCHT PCP iridium complexes, however with more possible isomers. Especially, the mass spectral characterisation of the iridium complexes reveals a substantial fragmentation pattern which was further investigated.

Therefore, a direct infusion set-up for electro-spray ionisation was developed allowing the sample injection with exclusion of air. The detailed exploration of the fragments, using density functional theory and mass spectrometry methods, illuminates a broad scope of CH-activation and hydrogen shift reactions between metal and ligand. Besides of the metal induced ligand degradation, adduct formation with nitrogen could be observed as well as the insertion of oxygen leading to an internal iridium oxo complex.

Acknowledgements

WL thanks the Deutsche Forschungsgemeinschaft (Graduiertenkolleg, Grant GK-GRK 441), Bonn/Bad Godesberg for financial support. We are indebted to Prof. W. C. Kaska whose generous support has been of value for many years. His special way of thinking about Chemistry has influenced many students who contributed to this and previous work of our groups.

Notes

^a Institute of Inorganic Chemistry, University of Tuebingen, Auf der Morgenstelle 18, 72076 Tuebingen, Germany. Fax: +49 7071 29 2436; Tel: +49 7071 29 76229; E-mail: hermann.mayer@uni-tuebingen.de.

^b Institut für Chemie - Bereich Anorganik, Karl-Franzens-Universität Graz, Schubertstr. 1, 8010 Graz, Austria; Present Address: EPCOS OHG, Siemensstr. 43, 8530 Deutschlandsberg, Austria; E-mail: johannes.wielandt@epcos.com.

Electronic Supplementary Information (ESI) available: structural details and comparisons of **9** and its CHT analogue, sketches of electro-spray infusion set-ups, overview of molecular fragments in the mass spectra, depicted calculated molecular structures, details to the calculation of energy differences, alternative bromination procedures and ³¹P monitoring of the formation of the oxo complex **16**. See DOI: 10.1039/b000000x/

References

- G. van Koten, *J. Organomet. Chem.*, 2013, **730**, 156–164.
- M. E. van der Boom and D. Milstein, *Chem Rev*, 2003, **103**, 1759–1792.
- D. Gelman and S. Musa, *ACS Catal.*, 2012, 2456–2466.
- A. Castonguay, A. L. Beauchamp, and D. Zargarian, *Organometallics*, 2008, **27**, 5723–5732.
- B. Vabre, M. L. Lambert, A. Petit, D. H. Ess, and D. Zargarian, *Organometallics*, 2012, **31**, 6041–6053.
- J. C. DeMott, N. Bhuvanesh, and O. V. Ozerov, *Chem. Sci.*, 2013, **4**, 642–649.
- D. Morales-Morales and C. M. Jensen, Eds., *The Chemistry of Pincer Compounds*, Elsevier, 2007.
- Organometallic Pincer Chemistry*, .
- S. Musa, I. Shaposhnikov, S. Cohen, and D. Gelman, *Angew. Chem. Int. Ed.*, 2011, **50**, 3533–3537.
- M. Vogt, A. Nerush, M. A. Iron, G. Leitus, Y. Diskin-Posner, L. J. W. Shimon, Y. Ben-David, and D. Milstein, *J. Am. Chem. Soc.*, 2013.
- H. Grützmacher, *Angew. Chem. Int. Ed.*, 2008, **47**, 1814–1818.
- S. Schneider, J. Meiners, and B. Askevold, *Eur. J. Inorg. Chem.*, 2012, **2012**, 412–429.
- J. I. van der Vlugt, M. Lutz, E. A. Pidko, D. Vogt, and A. L. Spek, *Dalton Trans*, 2009, 1016–1023.
- M. Vogt, O. Rivada-Wheelaghan, M. A. Iron, G. Leitus, Y. Diskin-Posner, L. J. W. Shimon, Y. Ben-David, and D. Milstein, *Organometallics*, 2012.
- A. Scharf, I. Goldberg, and A. Vignalok, *J. Am. Chem. Soc.*, 2012.
- J. Zhang, G. Leitus, Y. Ben-David, and D. Milstein, *J. Am. Chem. Soc.*, 2005, **127**, 10840–10841.
- C. Gunanathan and D. Milstein, *Acc. Chem. Res.*, 2011, **44**, 588–602.
- S. Nemeh, R. J. Flesher, K. Gierling, C. Maichle-Moessmer, H. A. Mayer, and W. C. Kaska, *Organometallics*, 1998, **17**, 2003–2008.
- A. M. Winter, K. Eichele, H.-G. Mack, W. C. Kaska, and H. A. Mayer, *Organometallics*, 2005, **24**, 1837–1844.
- A. M. Winter, K. Eichele, H.-G. Mack, W. C. Kaska, and H. A. Mayer, *Dalton Trans*, 2008, 527–532.
- W. Leis, H. A. Mayer, and W. C. Kaska, *Coord. Chem. Rev.*, 2008, **252**, 1787–1797.
- H. D. Beckey, *Angew. Chem. Int. Ed. Engl.*, 1969, **8**, 623–639.
- H. D. Beckey, H. Hey, K. Levsen, and G. Tenschert, *Int. J. Mass Spectrom. Ion Phys.*, 1969, **2**, 101–123.
- H. D. Beckey and H.-R. Schulten, *Angew. Chem. Int. Ed. Engl.*, 1975, **14**, 403–415.
- D. J. Surman and J. C. Vickerman, *J. Chem. Soc. Chem. Commun.*, 1981, 324–325.
- M. Barber, R. S. Bordoli, R. D. Sedgwick, and A. N. Tyler, *J. Chem. Soc. Chem. Commun.*, 1981, 325–327.
- C. Fenselau and R. J. Cotter, *Chem. Rev.*, 1987, **87**, 501–512.
- M. I. Bruce and M. J. Liddell, *Appl. Organomet. Chem.*, 1987, **1**, 191–226.
- J. M. Miller, *Mass Spectrom. Rev.*, 1990, **9**, 319–347.
- M. Dole, L. L. Mack, R. L. Hines, R. C. Mobley, L. D. Ferguson, and M. B. Alice, *J. Chem. Phys.*, 2003, **49**, 2240–2249.
- J. B. Fenn, M. Mann, C. K. Meng, S. F. Wong, and C. M. Whitehouse, *Mass Spectrom. Rev.*, 1990, **9**, 37–70.
- J. F. de la Mora, G. J. Van Berkel, C. G. Enke, R. B. Cole, M. Martinez-Sanchez, and J. B. Fenn, *J. Mass Spectrom.*, 2000, **35**, 939–952.
- G. J. V. B. and V. Kertesz, *Anal. Chem.*, 2007, **79**, 5510–5520.
- R. Colton, A. D'Agostino, and J. C. Traeger, *Mass Spectrom. Rev.*, 1995, **14**, 79–106.
- V. B. Di Marco and G. G. Bombi, *Mass Spectrom. Rev.*, 2006, **25**, 347–379.
- A. T. Lubben, J. S. McIndoe, and A. S. Weller, *Organometallics*, 2008, **27**, 3303–3306.
- L. Lepage and Y. Lepage, *Bull. Soc. Chim. Fr.*, 1988, 591–4.
- H. D. Kaesz and R. B. Saillant, *Chem. Rev.*, 1972, **72**, 231–281.
- A. M. Winter, Eberhard-Karls-Universität Tübingen, 2004.
- A. Vignalok, B. Rybtchinski, Y. Gozin, T. S. Koblenz, Y. Ben-David, H. Rozenberg, and D. Milstein, *J. Am. Chem. Soc.*, 2003, **125**, 15692–15693.
- M. E. van der Boom, T. Zubkov, A. D. Shukla, B. Rybtchinski, L. J. W. Shimon, H. Rozenberg, Y. Ben-David, and D. Milstein, *Angew. Chem. Int. Ed.*, 2004, **43**, 5961–5963.

42. S. Nemeh, C. Jensen, E. Binamira-Soriaga, and W. C. Kaska, *Organometallics*, 1983, **2**, 1442–7.
43. H. A. Y. Mohammad, J. C. Grimm, K. Eichele, H.-G. Mack, B. Speiser, F. Novak, M. G. Quintanilla, W. C. Kaska, and H. A. Mayer, *Organometallics*, 2002, **21**, 5775–5784.
44. F. Novak, B. Speiser, H. A. Y. Mohammad, and H. A. Mayer, *Electrochim Acta*, 2004, **49**, 3841–3853.
45. N. P. Tsvetkov, M. F. Laird, H. Fan, M. Pink, and K. G. Caulton, *Chem Commun*, 2009, 4578–4580.
46. P. Diversi, S. Iacoponi, G. Ingrosso, F. Laschi, A. Lucherini, and P. Zanello, *J Chem Soc Dalton Trans*, 1993, 351–352.
47. P. Diversi, S. Iacoponi, G. Ingrosso, F. Laschi, A. Lucherini, C. Pinzino, G. Uccello-Barretta, and P. Zanello, *Organometallics*, 1995, **14**, 3275–3287.
48. D. Conner, K. N. Jayaprakash, T. R. Cundari, and T. B. Gunnoe, *Organometallics*, 2004, **23**, 2724–2733.
49. T. B. Gunnoe, *Eur J Inorg Chem*, 2007, **2007**, 1185–1203.
50. L. N. Markovski and V. D. Romanenko, *Tetrahedron*, 1989, **45**, 6019–6090.
51. A. Jouaiti, M. Geoffroy, and G. Bernardinelli, *Tetrahedron Lett.*, 1993, **34**, 3413–3416.
52. D. J. Brauer, C. Liek, and O. Stelzer, *J. Organomet. Chem.*, 2001, **626**, 106–112.
53. R. Apfel, C. Casser, and F. Knoch, *J. Organomet. Chem.*, 1985, **293**, 213–217.
54. R. K. Harris, E. D. Becker, S. M. C. de Menezes, R. Goodfellow, and P. Granger, *Pure Appl. Chem.*, 2001, **73**, 1795–1818.
55. H. Hoffmann and P. Schellenbeck, *Chem Ber*, 1966, **99**, 1134–1142.
56. M. Fild, O. Stelzer, R. Schmutzler, and G. O. Doak, in *Inorg. Synth.*, eds. A. Wold and J. K. Ruff, McGraw-Hill Book Company, 1975, vol. 14.
57. *Jaguar, version 6.5-7.6*, Schrödinger, LLC, New York, NY, 2009.
58. *Maestro, version 7.5-9.0*, Schrödinger, LLC, New York, NY, 2009.
59. A. D. Becke, *J Chem Phys*, 1993, **98**, 5648–5652.
60. C. Lee, W. Yang, and R. G. Parr, *Phys Rev B*, 1988, **37**, 785–789.
61. P. J. Hay and W. R. Wadt, *J Chem Phys*, 1985, **82**, 299–310.
62. R. Ditchfield, W. J. Hehre, and J. A. Pople, *J Chem Phys*, 1971, **54**, 724–728.
63. W. J. Hehre and J. A. Pople, *J Chem Phys*, 1972, **56**, 4233–4234.
64. P. C. Hariharan and J. A. Pople, *Theor Chim Acta*, 1973, **28**, 213–222.
65. J. S. Binkley and J. A. Pople, *J Chem Phys*, 1977, **66**, 879–880.
66. M. M. Francl, W. J. Pietro, W. J. Hehre, J. S. Binkley, M. S. Gordon, D. J. DeFrees, and J. A. Pople, *J Chem Phys*, 1982, **77**, 3654–3665.
67. R. A. Friesner, R. B. Murphy, and M. N. Ringnalda, in *Encyclopedia of computational chemistry*, ed. P. R. von Schleyer, Wiley, 1998, vol. 3: M - P, pp. 2290–2300.

Graphical Abstract

Chemical conversions of a cycloheptatriene iridium pincer complex were studied by NMR and MS techniques as well as DFT calculations.

